

Direct measurement of the relative Fresnel (Goos-Hänchen) phase by polarization tomographySilvânia A. Carvalho ^{1,2,*}, Guilherme T. C. Cruz ², and Wagner F. Balthazar ^{2,3}¹*Escola de Engenharia Industrial Metalúrgica de Volta Redonda, Universidade Federal Fluminense, Volta Redonda, Rio de Janeiro, 27255-125, Brazil*²*Instituto de Ciências Exatas, Universidade Federal Fluminense, Volta Redonda, Rio de Janeiro, 27213-145, Brazil*³*Instituto Federal de Educação, Ciência e Tecnologia do Rio de Janeiro, IFRJ, Volta Redonda, Rio de Janeiro, 27213-100, Brazil*

(Received 13 July 2021; revised 9 November 2021; accepted 22 December 2021; published 13 January 2022)

In this work, we measure the relative Fresnel (Goos-Hänchen) phase, which is acquired after beam propagation through a two-phase ellipsometric system under total internal reflection, by using polarization tomography. This approach presents a direct measurement which provides a more powerful and complete description of the polarization state. In this sense, the relative phase can be obtained through the polarization-state reconstruction. The experimental data confirm the simulated intensity profiles and allow us to access information about the amplitude and relative phase of the polarization state instead of measuring phase effects.

DOI: [10.1103/PhysRevA.105.013515](https://doi.org/10.1103/PhysRevA.105.013515)**I. INTRODUCTION**

Studies on deviations from the Snell's law prediction have received considerable attention since Goos and Hänchen's observations [1,2] and Artman's theoretical predictions [3]. While some researchers were using their best efforts to measure this very tiny beam displacement [4], other researchers investigated these optical beam shifts theoretically [5–13], improving community knowledge about the effect amplification. It is worth mentioning that deepening of the topic led to the discovery of new phenomena such as the asymmetric Goos-Hänchen (GH) shift [14], angular GH shift [15–18], composite GH shift [19–21], GH shift for partially coherent light beams [22], GH shift in the Floquet scattering of Dirac fermions [23], GH shift in physical systems such as the optomechanical cavity and metal-clad waveguide structure [24,25], and so on. To focus on the principal challenge of beam-shift amplification, new physical systems were investigated by using the physical properties of multiple reflections, weak measurements, Bloch surface wave excitation, symmetrical metal-cladding waveguides, and medium absorption, among others [1,19,22,26–31].

Following the main idea of exploring new systems, recent studies demonstrated that propagation of a linearly polarized light composed of transverse electric (TE) and transverse magnetic (TM) components at the dielectric-air interface under total reflection leads to a relative Fresnel Goos-Hänchen [F(GH)] phase between the orthogonal states which produces power oscillations [32–34]. To explore this relative phase, some researchers use the main idea behind the ellipsometry technique [35–41], i.e., the optical phase difference provided by the polarization-sensitive response of the physical system to change the linearly polarized beam into a reflected elliptically polarized beam upon the reflection condition. In general,

investigations of lateral beam shifts due to the GH phase are done through measurements of the location of the beam's intensity peak [21], photoemission electron microscopy images [42], and weak measurements with compensation of the relative F(GH) phase by using zero-order half- (HWP) and quarter- (QWP) wave plates [19,26–28]. It is worth mentioning that the direct measure of the GH phase was done only for microwave optics and quantum systems [43,44].

In our contribution, the main idea is to determine this F(GH) relative phase by applying the polarization tomography to the output beam emerging from the complex GH ellipsometric system composed of a dielectric medium with real refractive index n , as proposed in [32]. The main advantages of this approach are the determination of the relative F(GH) phase, instead of beam displacement, and the possibility to investigate other degrees of freedom of the electromagnetic field [45]. To the best of our knowledge, polarization tomography has not been used before in this context. The use of polarization tomography allows us to access this relative phase between orthogonal waves without any kind of interference measurement, which was not possible at one time because states polarized in linearly independent directions do not interfere in interferometry. It is important to mention that our approach is a classical counterpart of quantum tomography [46]. The approach is possible due to the similarity between the mathematical structure of the quantum states and the degrees of freedom of the electromagnetic field since both can be described by complex vector spaces. For example, in classical optics, any polarization vector can be described as a complex superposition of circularly polarized light, similar to the spin of a quantum particle. In this scenario, many works have studied quantum systems with the degrees of freedom of an intense laser beam [47–50], and in some works the state is completely characterized by performing quantum state tomography in an all-classical optical setup [50,51]. In our work, we use this approach to reconstruct the laser-beam polarization via tomography by using an optical circuit.

*silvaniaalves@id.uff.br

Therefore, the direct measurement of the relative F(GH) phase can be performed for any physical system, independent of the geometrical layout, by acquiring the output intensities of the tomography optical circuit.

This paper is organized as follows. In Sec. II, we present a basic description of the F(GH) relative phase together with a brief introduction to the quantum tomography technique which will be employed in the relative phase investigation. In particular, the analogy between optics and quantum mechanics is applied to optical beams upon reflection to determine the F(GH) relative phase in Sec. III. In the sequence, the quantum tomography not only reconstructs the quantum state but also confirms the F(GH) relative phase predictions in Sec. IV. In addition, we present theoretical and experimental beam intensities for beams upon reflection which can be observed in an implementation of polarization tomography to estimate the relative F(GH) phase. Finally, we conclude our contribution with the main results and future perspectives in Sec. V.

II. THEORETICAL APPROACH

In what follows, we present the physical system and the theoretical approach required to describe the relative F(GH) phase acquired by beam propagation through a complex GH ellipsometric system [32].

A. The relative Fresnel (GH) phase

For our proposal, after propagation in free space, the incoming beam encounters the polarizer $P_{\pi/4}$, which selects the incident polarization state with an angle $\pi/4$, i.e., the linearly polarized beam composed of TE and TM components,

$$\mathcal{E}_{\text{inc}}(\mathbf{r}) = \begin{bmatrix} E_x(\mathbf{r}) \\ E_y(\mathbf{r}) \end{bmatrix} = E(\mathbf{r}) \begin{bmatrix} 1 \\ 1 \end{bmatrix}, \quad (1)$$

where

$$E(\mathbf{r}) = \frac{E_0}{\sqrt{1 + iz/z_r}} \exp\left[-\frac{x^2 + y^2}{w_0^2(1 + iz/z_r)}\right] \quad (2)$$

and $z_r = \pi w_0^2/\lambda$. Here, w_0 is the beam waist size, and λ is the wavelength. The incoming beam $\mathcal{E}_{\text{inc}}(\mathbf{r})$ hits the dielectric structures composed of N ($= 1, 2, 3, 4$) barium borosilicate (BK7) ($n = 1.5195$ at $\lambda = 532$ nm) blocks at an incidence angle θ which respects the relations $\sin \theta = n \sin \psi$ and $\varphi = \pi/4 + \psi$, with ψ being the angle of the refracted beam and φ being the angle of incidence at the down dielectric-air interface. AB and BC are the left and right and lower and upper dielectric interfaces [see Fig. 1(a)].

Under total internal reflection, the F(GH) phase appears in the Fresnel coefficient when $n \sin \varphi \geq 1$, i.e., for the angle $\theta \geq -5.847^\circ$ ($\varphi \geq 41.156^\circ$). For these conditions, the Fresnel transmission coefficients for TE and TM waves are given by

$$T_\sigma = \left[\frac{4 a_\sigma \cos \theta \cos \psi}{(a_\sigma \cos \theta + \cos \psi)^2} \right]^N \exp[i \Phi_\sigma], \quad (3)$$

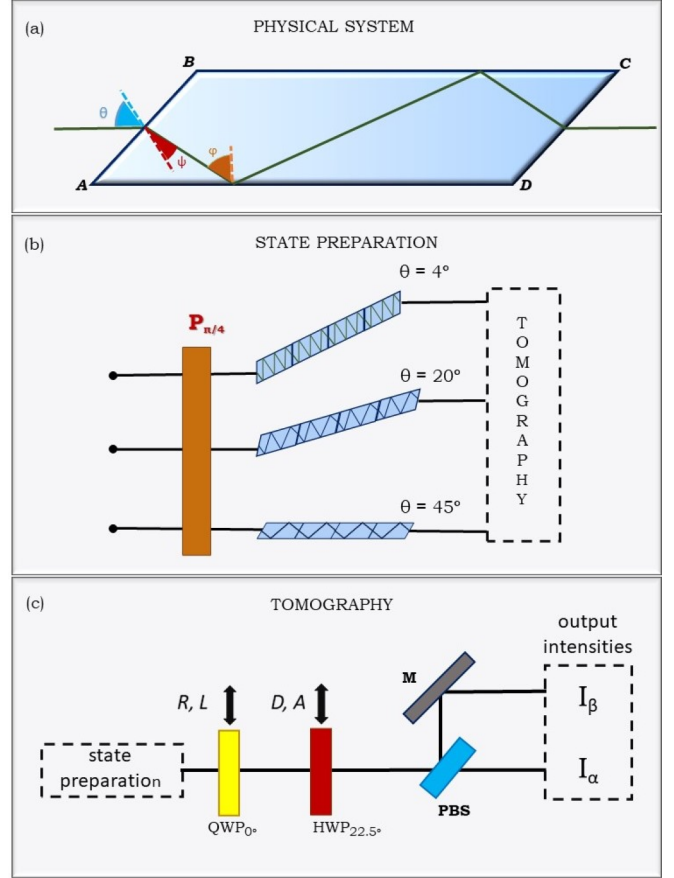


FIG. 1. Physical system. In (a), the planar view of the BK7 block shows the geometrical system in which θ is the angle of incidence, ψ is the angle of the refracted beam, and φ is the angle of incidence at the down dielectric-air interface. In (b), the free incoming beam is mixed by the polarizer ($P_{\pi/4}$) located before the dielectric structure. Here, three incidence-angle values of 4° , 20° , and 45° are employed to increase the number of reflection N_{ref} and the acquired F(GH) phase. After state preparation, the elliptical polarized light goes to the quantum tomography system in (c) composed of a quarter-wave plate (QWP), a half-wave plate (HWP), and a polarized beam splitter (PBS).

in which $\sigma = \{\text{TE}, \text{TM}\}$, $\{a_{\text{TE}}, a_{\text{TM}}\} = \{1/n, n\}$, and

$$\Phi_\sigma = -2 N_{\text{ref}} \arctan \left[a_\sigma \frac{\sqrt{n^2 \sin^2 \varphi - 1}}{\cos \varphi} \right] \quad (4)$$

is the F(GH) phase for TE and TM components. For the same BK7 block dimensions as in Ref. [34]

$$\underbrace{(91.5) \text{ mm}}_{BC} \times \underbrace{(20.0) \text{ mm}}_{AB} \times (14.0) \text{ mm},$$

we assume $N_{\text{ref}} = 2, 4, 6$ is the number of internal reflections for the chosen angles $\theta = 4^\circ, 20^\circ, 45^\circ$, as illustrated in Fig. 1(b). It is worth mentioning that the geometrical phase, also known as the Snell phase ϕ_{Snell} , provided by the continuity conditions at each air-dielectric (dielectric-air) interface, is the same for TE and TM waves [32,34]. Due to the fact that the first-order contribution of the GH-phase expansion leads to beam-displacement terms x_σ which can be neglected in comparison with the first-order contribution of the Snell

phase x_{Snell} , the state preparation provided the output beam

$$\mathcal{E}_{\text{tra}}(\mathbf{r}) \approx E(x - x_{\text{Snell}}, y, z) \exp[i\Phi_{\text{Snell}}] \times \begin{bmatrix} |T_{\text{TM}}| \exp[i\Phi_{\text{TM}}] \\ |T_{\text{TE}}| \exp[i\Phi_{\text{TE}}] \end{bmatrix}. \quad (5)$$

Because we are interested in the relative F(GH) phase, we can neglect the Snell term in our calculation. After a few algebraic calculations, we can simplify the above expression to obtain

$$\mathcal{E}_{\text{tra}}(\mathbf{r}) \approx \begin{bmatrix} 1 \\ \tau \exp[i\Delta_{\text{F(GH)}}] \end{bmatrix}, \quad (6)$$

with

$$\tau = \left| \frac{T_{\text{TE}}}{T_{\text{TM}}} \right| = \left(\frac{n \cos \theta + \cos \psi}{\cos \theta + n \cos \psi} \right)^{2N} \quad (7)$$

and

$$\Delta_{\text{F(GH)}} = \Phi_{\text{TE}} - \Phi_{\text{TM}} = 2N_{\text{ref}} \arctan \left[\frac{\sqrt{n^2 \sin^2 \varphi - 1}}{n \sin \varphi \tan \varphi} \right], \quad (8)$$

which is the relative phase between TE and TM components. References [32,34] used a second polarizer to mix the TE and TM waves with an angle $\pi/4$ in order to observe oscillations in the power of the transmitted beam. In our contribution, we replace the polarizer by a quantum tomography technique which is applied to the outgoing beam emerging from the state preparation in order to reconstruct the quantum state and to determine the relative F(GH) acquired after propagation through the dielectric structure.

B. Polarization tomography

In order to characterize all prepared polarization states shown in Fig. 1(b), we use the optical circuit sketched in Fig. 1(c) to perform the polarization tomography and reconstruct the polarization state in the density-matrix formalism, which can be completely described by the Stokes parameters S_i [46],

$$\rho = \frac{1}{2} \sum_{i=1}^3 S_i \hat{\sigma}_i, \quad (9)$$

where $i = 0, 1, 2, 3$ are associated with the polarization modes and $\hat{\sigma}_i$ are the Pauli matrices. The parameters S_i can be obtained by a specific pair of outcome projective measurements as follows: $S_0 = P_H + P_V$, $S_1 = P_D - P_A$, $S_2 = P_R - P_L$, and $S_3 = P_H - P_V$. P is the probability of the state being projective in specific bases labeled the $\{H, V\}$ (or $\{\text{TE}, \text{TM}\}$) basis, diagonal basis $\{D, A\}$, and circular basis $\{R, L\}$.

It is important to mention that we are exploring the similarity between the mathematical structure of the polarization state of the electromagnetic field and the quantum state vector. In this sense, we have adopted the quantum mechanics formalism to describe the polarization state of a classical beam and its tomography. In this scenario, the probabilities P from Stokes parameters S_i are associated with the laser-beam normalized intensities I_α/I_T and I_β/I_T [Fig. 1(c)], where α and β correspond to the $\{H, D, R\}$ and $\{V, A, L\}$ bases, respectively, and $I_T = I_\alpha + I_\beta$.

TABLE I. Theoretical prediction for the outgoing beam $\mathcal{E}_{\text{tra}}(\mathbf{r})$ which emerges from the state-preparation stages for different incidence angles and dielectric blocks configurations.

θ (deg)	N	$\mathcal{E}_{\text{tra}}(\mathbf{r})$
4	1	[1, (0.00309 - 0.99942j)]
	2	[1, (-0.99884 - 0.00618j)]
	3	[1, (-0.00927 + 0.99825j)]
	4	[1, (0.99764 + 0.01235j)]
20	1	[1, (-0.97570 + 0.13638j)]
	2	[1, (0.93339 - 0.26613j)]
	3	[1, (-0.87441 + 0.38696j)]
	4	[1, (0.80039 - 0.49680j)]
45	1	[1, (0.57673 + 0.70636j)]
	2	[1, (-0.16632 + 0.81476j)]
	3	[1, (-0.67144 + 0.35242j)]
	4	[1, (-0.63618 - 0.27103j)]

In Fig. 1(c), we present the optical tomography block. The S_0 or S_3 parameters can be obtained by performing projective measurements in the $\{H, V\}$ basis using a PBS. In the same way, the PBS associated with the half-wave plate ($\text{HWP}_{22.5^\circ}$) performs projective measurements in the diagonal basis $\{D, A\}$ in order to obtain the S_1 parameter. Finally, the sequence of a quarter-wave plate (QWP_{0°) with $\text{HWP}_{22.5^\circ}$ and the PBS correspond to the right- and left-handed circular polarization basis $\{R, L\}$. Therefore, we can compute all Stokes parameters S_i measuring the output intensities (I_α, I_β) in order to reconstruct the density matrix presented in Eq. (9).

III. THE RELATIVE (FRESNEL) GH-PHASE PREDICTIONS

After passing through the state-preparation stage, the outgoing beam $\mathcal{E}_{\text{tra}}(\mathbf{r})$ will be a source of systems for the quantum state tomography, as described in Sec. II B. By applying the polarization tomography to this source, we are able to determine the quantum state, i.e., to obtain a complete description of the polarization state based on the amplitude and relative F(GH) phase. Note that this will provide the same result predicted by the analogy between optics and quantum mechanics in Eqs. (7) and (8). In Table I, we show the predictions from Eq. (6) for incidence angles equal to $\theta = 4^\circ, 20^\circ, 45^\circ$ and $N = 1, 2, 3, 4$.

Our analytical expression for the relative F(GH) phase, Eq. (8), leads to the theoretical predictions presented in the third column of Table II for the same conditions as in Table I. In the next section we describe how to obtain the relative F(GH) phase by applying the quantum tomography to the quantum states, i.e., the outgoing beams $\mathcal{E}_{\text{tra}}(\mathbf{r})$ emerging from the state preparation.

IV. SIMULATED AND EXPERIMENTAL RESULTS

In this section, we present the theoretical and experimental results of the optical tomography process [Fig. 1(c)] for the input polarization states presented in Table I.

TABLE II. Theoretical prediction for the relative F(GH) phase $\Delta_{\text{F(GH)}}$ for beam propagation under total reflection. The third column provides results for Eq. (8), and the last column presents the quantum tomography results.

θ (deg)	N	$\Delta_{\text{F(GH)}}$	$\Delta_{\text{F(GH),tomo}}$
4	1	4.7155	4.7155
	2	9.4310	9.4310
	3	14.1465	14.1465
20	4	18.8619	18.8619
	1	3.0027	3.0027
	2	6.0054	6.0054
45	3	9.0081	9.0081
	4	12.0109	12.0109
	1	0.8861	0.8861
	2	1.7722	1.7722
	3	2.6582	2.6582
	4	3.5443	3.5443

A. Simulation of the polarization tomography and phase estimation

First, in order to exemplify, we present the simulated output intensities (Fig. 2) for $\theta = 4^\circ$ and one block ($N = 1$) considering the experimental setup in Fig. 1. Columns P_α and P_β correspond to the output normalized intensities for all bases, $P_\alpha = I_\alpha / (I_\alpha + I_\beta)$ and $P_\beta = I_\beta / (I_\alpha + I_\beta)$, and column N is the number of blocks in the physical system. The columns labeled P_H and P_V are related to the measurements in the $\{H, V\}$ (or $\{TE, TM\}$) basis. In this case, the tomography circuit is reduced to a PBS. Note that for a different number of blocks N , the output intensities are very similar, which happens because the state polarization of the laser beam \mathcal{E}_{tra} can be considered to be practically circularly polarized for $N = 1$ and 3 and diagonally polarized for $N = 2$ and 4, as shown in Table I. However, when tomography measurements are performed in the diagonal basis $\{D, A\}$, i.e., with a PBS coupled with $\text{HWP}_{22.5^\circ}$, as shown in Fig. 1(c), the behavior

N	P_H	P_V	P_D	P_A	P_R	P_L
1	0.5003	0.4997	0.5015	0.4985	0.0000	1.0000
2	0.5006	0.4994	0.0000	1.0000	0.4969	0.5031
3	0.5009	0.4991	0.4954	0.5046	1.0000	0.0000
4	0.5011	0.4989	1.0000	0.0000	0.5062	0.4938

FIG. 2. Simulated output hot-color images for the optical tomography circuit.

is different; as we can see in the P_D and P_A columns the output normalized intensities are off for $N = 2$ and 4, respectively. This occurs because the state corresponding to $N = 2$ has antidiagonal polarization ($P_D = 0.0000$ and $P_A = 1.0000$) and the state corresponding to $N = 4$ has diagonal polarization ($P_D = 1.0000$ and $P_A = 0.0000$), exactly as we expected. When the laser beam is circularly polarized ($N = 1$ and 3), the output normalized intensities are close to 0.5000, also as we expected. In the same way, the P_R and P_L columns correspond to the measures in the circular basis $\{R, L\}$, which is performed by adding QWP_{0° to the previous description. In this sense, we use all optical devices presented in Fig. 1(c). For circular polarization ($N = 1$ and 3), the intensities' outputs are $P_R = 0.0000$ and $P_L = 1.0000$ ($P_R = 1.0000$ and $P_L = 0.0000$) for right (left) circular polarization. For diagonal polarization ($N = 2$ and 4), the output normalized intensities are close to 0.5000.

Now, P_α and P_β can be used to evaluate the Stokes parameters S_i [46]. For example, for the state after one block ($N = 1$), we obtain $S_0 = 0.5003 + 0.4997$, $S_1 = 0.5015 - 0.4985$, $S_2 = 0.000 - 1.000$, and $S_3 = 0.5003 - 0.4997$. Therefore, we can compute the density matrix ρ , Eq. (9), to obtain

$$\rho_{\text{sim}} = \begin{pmatrix} 0.5003 & 0.0015 + 0.5000j \\ 0.0015 - 0.5000j & 0.4997 \end{pmatrix}. \quad (10)$$

As we expected, this is a pure state since ρ is Hermitian, $\rho^2 = \rho$, and $\text{tr}(\rho^2) = 1$. Consequently, we can recover the state using $\rho = |E_{\text{tra}}\rangle \langle E_{\text{tra}}|$ in order to obtain the simulated polarization state in the vector formalism, given by $|E_{\text{tra}}\rangle_{\text{sim}} = [0.7073, (0.0021 - 0.7069j)]$ for $\theta = 4^\circ$ and $N = 1$. This state is exactly the same as presented in Table I with one single difference: here, the vector is normalized. The F(GH) phase evaluated for this state, $\Delta_{\text{F(GH),tomo}} = 4.7155$, corresponds to theoretical prediction, as shown in Table II.

By performing the polarization tomography for all states presented in Table I, we obtain all corresponding output intensities. In this sense, we can calculate the Stokes parameters and recover all states presented in Table I. So the F(GH) phase was calculated for different angles θ and different numbers of blocks N , as shown in Table II.

As can be observed, all values $\Delta_{\text{F(GH),tomo}}$ presented are in excellent agreement with the theoretical predictions. Consequently, we show that polarization tomography is an effective technique to evaluate the Goos-Hänchen phase for any dielectric structure since we do not need to specify the geometrical layout.

B. Experimental results for the F(GH) relative phase by polarization tomography

In this section, we present the experimental results obtained for the optical setup sketched in Fig. 1. A diode-pump solid-state (DPSS) laser beam (532 nm and 0.4 μW) that is diagonally polarized is used as an incident polarized input state on the BK7 block ($n = 1.5195$ at $\lambda = 532$ nm). The experiment is performed using one ($N = 1$), two ($N = 2$), and three blocks ($N = 3$) in sequence [Fig. 1(b)] and the polarization tomography system [Fig. 1(c)] to obtain the output


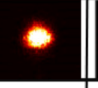
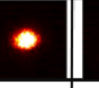
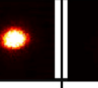
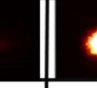

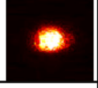
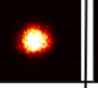
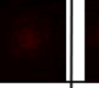
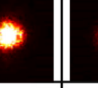
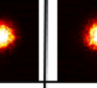
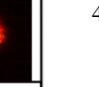
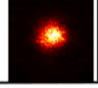
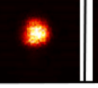
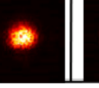
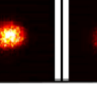
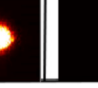

N	P_H	P_V	P_D	P_A	P_R	P_L
1	0.5003	0.4997	0.4788	0.5212	0.0090	0.9910
						
2	0.4818	0.5182	0.0157	0.9843	0.4509	0.5491
						
3	0.4646	0.5354	0.4938	0.5062	0.9923	0.0077
						

FIG. 3. Experimental output hot-color images for the optical tomography circuit.

intensities, which are obtained by recording them with a CCD camera.

Figure 3 shows the experimental output normalized intensities (P_α and P_β) of the tomography for the preselected basis, $\theta = 4^\circ$, and one block ($N = 1$), which should be contrasted with the simulated results presented in Fig. 2. As we can see, all experimental intensities are in very good agreement with the simulated results (see Fig. 3). Just a slight difference can be noticed, which occurs because of the errors in the optical devices. For example, the PBS has a visibility around 98% for the 532-nm vertical polarized laser beam. It is also important to highlight that the intensities decrease when we add BK7 blocks (N) to the experimental setup, which occurs mainly due to the coating losses in each reflection and transmission. Note that the intensity decrease does not affect our results because the intensities must be normalized to determine the density matrix.

As in the previous section, we use P_α and P_β to evaluate the Stokes parameters S_i [46]. For the state after one block ($N = 1$), we obtain $S_0 = 0.5003 + 0.4997$, $S_1 = 0.4788 - 0.5212$, $S_2 = 0.0009 - 0.9910$, and $S_3 = 0.5003 - 0.4997$. Therefore, we can compute the density matrix ρ , Eq.(9), to obtain

$$\rho_{\text{exp}} = \begin{pmatrix} 0.5003 & -0.0212 + 0.4910j \\ -0.0212 - 0.4910j & 0.4997 \end{pmatrix}. \quad (11)$$

Comparing the density matrices in Eqs. (10) and (11), we see that they are similar. The diagonals of both matrices are equal, and the antidiagonals have small differences in the second and third decimal places. Accordingly, we obtain the polarization state $|E_{\text{tra}}\rangle_{\text{exp}} = [0.7073, (-0.0299 - 0.6942j)]$, which is similar to the previous polarized state $|E_{\text{tra}}\rangle_{\text{sim}}$. The F(GH) phase evaluated for this state, $\Delta_{\text{F(GH),tomo}}^{\text{exp}} = 4.6693$, corresponds to the experimental result, which has an error of 0.98% compared to the simulated value. Table III shows the experimental results for different angles of incidence θ and different numbers of blocks N .

In all present results, the relative F(GH) phases obtained experimentally $\Delta_{\text{F(GH),tomo}}^{\text{exp}}$ are in very good agreement with the theoretical prediction $\Delta_{\text{F(GH),tomo}}^{\text{theo}}$. The last column of Ta-

TABLE III. Theoretical and experimental prediction for the relative F(GH) phase $\Delta_{\text{F(GH)}}$ for beam propagation under total reflection. The third column provides theoretical results for polarization tomography, the fourth column presents the experimental tomography results, and the last column illustrates the percent error.

θ (deg)	N	$\Delta_{\text{F(GH),tomo}}^{\text{theo}}$	$\Delta_{\text{F(GH),tomo}}^{\text{exp}}$	Error (%)
4	1	4.7155	4.6693	0.98
	2	9.4310	9.3238	1.14
	3	14.1465	14.1498	0.02
20	1	3.0027	2.9656	1.24
	2	6.0054	5.9341	1.19
	3	9.0081	8.8196	2.09
45	1	0.8861	0.8621	2.71
	2	1.7722	1.7081	3.62
	3	2.6582	2.7096	1.93

ble III reveals small deviations between the theoretical and experimental values of the relative F(GH) phases. These deviations are typical in the optical experimental setups.

V. CONCLUSIONS

In conclusion, we investigated the direct measurement of the relative F(GH) phase by applying a complete and more powerful tool, polarization tomography. The intensity profiles generated by the experimental tomography optical circuit showed that all information concerning the polarization state can be accessed. Furthermore, all simulated and experimental results are in excellent agreement with the theoretical predictions.

To the best of our knowledge, polarization tomography has not been used before in this context for the relative F(GH) phase determination. This approach offers the advantage of providing a complete description of the optical beam (amplitude and relative phase) through a simple optical system which reconstructs the polarization state. As a consequence, this technique is of great importance to estimate the relative phase as well as the weak measurement of quantum mechanics was essential in the GH shift measurement.

It is worth noting that the tomography process can also be applied to other degrees of freedom of the electromagnetic field, such as the transverse mode (Hermite or Laguerre beams) and path. In this scenario, application of the tomography process to this research area involving optical beam shifts opens possibilities for future investigations.

ACKNOWLEDGMENTS

We would like to thank the Brazilian funding agencies Fundação Carlos Chagas Filho de Amparo à Pesquisa do Estado do Rio de Janeiro (FAPERJ; No. E-26/010/002464/2019 (Ref. 211.599/2019), No. E-26/110.218/2011, and No. E-26/211.109/2019) and the Brazilian National Institute for Science and Technology of Quantum Information (INCT-IQ) for financial support. We also thank the Conselho Nacional de Desenvolvimento Científico e Tecnológico (CNPq) for the scholarships (PIBIC/UFF 2020-2021) of G.T.C.C. and Project No. 429990/2018-9.

- [1] F. Goos and H. Hänchen, *Ann. Phys. (Berlin, Ger.)* **436**, 333 (1947).
- [2] F. Goos and H. Hänchen, *Ann. Phys. (Berlin, Ger.)* **440**, 251 (1949).
- [3] K. Artmann, *Ann. Phys. (Berlin, Ger.)* **437**, 87 (1948).
- [4] F. Bretenaker, A. Le Floch, and L. Dutriaux, *Phys. Rev. Lett.* **68**, 931 (1992).
- [5] B. R. Horowitz and T. Tamir, *J. Opt. Soc. Am.* **61**, 586 (1971).
- [6] K. Y. Bliokh and A. Aiello, *J. Opt.* **15**, 014001 (2013).
- [7] A. Aiello and J. P. Woerdman, *Opt. Lett.* **33**, 1437 (2008).
- [8] M. P. Araújo, S. A. Carvalho, and S. De Leo, *J. Mod. Opt.* **60**, 1772 (2013).
- [9] M. P. Araújo, S. De Leo, and G. Maia, *Phys. Rev. A* **93**, 023801 (2016).
- [10] S. A. Carvalho and S. De Leo, *Am. J. Phys.* **83**, 249 (2015).
- [11] S. Longhi, G. D. Valle, and K. Staliunas, *Phys. Rev. A* **84**, 042119 (2011).
- [12] Ziauddin and S. Qamar, *Phys. Rev. A* **84**, 053844 (2011).
- [13] Ziauddin and S. Qamar, *Phys. Rev. A* **85**, 055804 (2012).
- [14] M. P. Araújo, S. A. Carvalho, and S. De Leo, *J. Opt.* **16**, 015702 (2014).
- [15] M. P. Araújo, S. A. Carvalho, and S. De Leo, *Phys. Rev. A* **90**, 033844 (2014).
- [16] M. P. Araújo, S. De Leo, and G. Maia, *J. Opt.* **17**, 035608 (2015).
- [17] M. P. Araújo, S. De Leo, and G. G. Maia, *Ann. Phys. (Berlin, Ger.)* **529**, 1600357 (2017).
- [18] S. De Leo and G. G. Maia, *J. Mod. Opt.* **66**, 2142 (2019).
- [19] O. Santana, S. A. Carvalho, S. De Leo, and L. E. E. de Araujo, *Opt. Lett.* **41**, 3884 (2016).
- [20] M. P. Araújo, S. De Leo, and G. G. Maia, *Phys. Rev. A* **95**, 053836 (2017).
- [21] O. Santana and L. E. E. de Araujo, *Opt. Lett.* **43**, 4037 (2018).
- [22] O. Santana and L. E. E. de Araujo, *J. Opt. Soc. Am. B* **36**, 533 (2019).
- [23] A. Huamán and G. Usaj, *Phys. Rev. A* **100**, 033409 (2019).
- [24] A. A. Khan, M. Abbas, Y. L. Chaung, I. Ahmed, and Ziauddin, *Phys. Rev. A* **102**, 053718 (2020).
- [25] R.-G. Wan and M. S. Zubairy, *Phys. Rev. A* **101**, 023837 (2020).
- [26] M. R. Dennis and J. B. Götze, *New J. Phys.* **14**, 073013 (2012).
- [27] G. Jayaswal, G. Mistura, and M. Merano, *Opt. Lett.* **38**, 1232 (2013).
- [28] G. Jayaswal, G. Mistura, and M. Merano, *Opt. Lett.* **39**, 6257 (2014).
- [29] Y. Wan, Z. Zheng, W. Kong, X. Zhao, Y. Liu, Y. Bian, and J. Liu, *Opt. Express* **20**, 8998 (2012).
- [30] L. Chen, Z. Cao, F. Ou, H. Li, Q. Shen, and H. Qiao, *Opt. Lett.* **32**, 1432 (2007).
- [31] W. J. Wild and C. L. Giles, *Phys. Rev. A* **25**, 2099 (1982).
- [32] M. P. Araújo, S. De Leo, and G. Maia, *Chin. Opt. Lett.* **16**, 031406 (2018).
- [33] M. P. Araújo, S. De Leo, and G. Maia, *Eur. Phys. J. D* **73**, 213 (2019).
- [34] S. A. Carvalho, S. De Leo, J. A. O. Huguenin, M. Martino, L. da Silva, *Laser Phys. Lett.* **16**, 065001 (2019).
- [35] M. Losurdo, M. Bergmair, G. Bruno, D. Cattelan, C. Cobet, A. de Martino, K. Fleischer, Z. Dohcevic-Mitrovic, N. Esser, M. Galliet, R. Gajic, D. Hemzal, K. Hingerl, J. Humlicek, R. Ossikovski, Z. V. Popovic, and O. Saxl, *J. Nanopart. Res.* **11**, 1521 (2009).
- [36] H. Fujiwara, *Spectroscopic Ellipsometry: Principles and Applications* (Wiley, Tokyo, 2003).
- [37] L. F. N. Guedes, M. T. D. Garcia, J. N. Cunha, L. T. Duarte, D. Bertagnolli, L. da Silva, J. A. O. Huguenin, and E. A. Ferreira, *J. Solid State Electrochem.* **20**, 2517 (2016).
- [38] L. Arsov and I. Mickova, *J. Electrochem. Sci. Eng.* **5**, 221 (2015).
- [39] S. Joo, I. Muto, and N. Hara, *J. Electrochem. Soc.* **155**, C154 (2008).
- [40] K. Vedam, *Thin Solid Films* **313–314**, 1 (1998).
- [41] D. E. Aspnes, *Thin Solid Films* **571**, 334 (2014).
- [42] T. Stenmark, R. C. Word, and R. Könenkamp, *Opt. Express* **24**, 3839 (2016).
- [43] L. Arthur, A. Read, I. R. Dagg, and G. E. Reesor, *Can. J. Phys.* **50**, 52 (1972).
- [44] J. H. Shapiro and S. R. Shepard, *Phys. Rev. A* **43**, 3795 (1991).
- [45] Z. Zhu, D. Hay, Y. Zhou, A. Fyffe, B. Kantor, G. S. Agarwal, R. W. Boyd, and Z. Shi, *Phys. Rev. Appl.* **12**, 034036 (2019).
- [46] J. B. Altepeter, E. R. Jeffrey, and P. G. Kwiat, *Adv. At. Mol. Opt. Phys.* **52**, 105 (2005).
- [47] K. H. Kagalwala, G. Di Giuseppe, A. F. Abouraddy, and B. E. Saleh, *Nat. Photonics* **7**, 72 (2013).
- [48] C. V. S. Borges, M. Hor-Meyll, J. A. O. Huguenin, and A. Z. Khoury, *Phys. Rev. A* **82**, 033833 (2010).
- [49] W. F. Balthazar, C. E. R. Souza, D. P. Caetano, E. F. Galvão, J. A. O. Huguenin, and A. Z. Khoury, *Opt. Lett.* **41**, 5797 (2016).
- [50] W. F. Balthazar, D. G. Braga, V. S. Lamego, M. H. M. Passos, and J. A. O. Huguenin, *Phys. Rev. A* **103**, 022411 (2021).
- [51] M. H. M. Passos, A. C. Santos, M. Sarandy, and J. A. O. Huguenin, *Phys. Rev. A* **100**, 022113 (2019).